International Journal of Advanced Research in Chemical Science (IJARCS)
Volume 2, Issue 7, July 2015, PP 7-21
ISSN 2349-039X (Print) & ISSN 2349-0403 (Online)
www.arcjournals.org

Synthesis Properties and Electrocatalytic Activities of Pd, Ru, Rh Nanoparticles

A.A. Revina[1,2], M.A. Kuznetsov[2], S.A. Busev[1], E.E. Boyakov[1], A.A. Mikhaylov[2], A.M. Chekmarev[1,2]

[1]Institution of Russian Academy of Sciences
A.N. Frumkin Institute of Physical Chemistry and Electrochemistry RAS
[2]D. Mendeleyev Russian University of Chemical Technology Moscow,
Russia, Miusskaya sc.
alex_revina@mail.ru, mikhael.kuznetsov@gmail.com

1. INTRODUCTION

The increasing of the radiation chemistry role in the field of fundamental and applied research in modern nanotechnologies obvious and is connected with its high potential in the study of the mechanism of oxidation-reduction reactions in homogeneous and heterogeneous systems under interaction of various physical and chemical factors. Radiation chemistry has the great opportunities in the creation of nanostructured ensembles with specified properties when used the reverse micellar solutions as micro reactor. The advantage of this method is the stability of nanoparticles in a liquid phase and in the adsorbed state, the possibility to use the different physical-chemical methods for studying the properties of nanoparticles in a liquid phase: UV-VIS spectrophotometry, luminescent analysis, HPLC and photon correlation spectroscopy. The obtained results confirm – the formation, the nanoparticles stability, their evolution (under controlled and specified conditions), the functional activity not only themselves nanostructures and supramolecular ensembles, but also bimetallic particles and polymeric nanocomposite materials.

2. PROPERTIES AND APPLICATION OF PD, RU, RH METAL NANOPARTICLES

2.1. Pd Nanoparticles Using in Chemical Catalysis

Palladium catalysts are used in many processes of organic synthesis. The characteristics improvement of the catalysts, and reducing the palladium is due to using of palladium nanoparticles at the creation of nanocomposites.

Study of the adsorption properties of palladium nanoparticles, NP, on the silica gel and the surface of many other materials has created the nanocomposite materials with high activity. Thus, when using a porous ceramic honeycomb material, modified by palladium nanoparticles, was found to be high catalytic activity and increased selectivity to the desired product in the methylation reaction of aniline with formaldehyde to monomethylaniline in liquid phase [14].

2.2. Pd Nanoparticles in Fuel Cells

Creation of new catalytic systems for low temperature fuel cells anodes mainly focused on the use of Pd nanoparticles. The nanocomposites with Pd NP used as anodes in the electrocatalytical reactions for fuel cells primarily because palladium is resistant to CO, the main catalytic poison for hydrogen fuels. Formic acid is one of the most promising fuels for micropower current sources. In the fuel cell the anode reaction oxidation of HCOOH is carried out directly without an intermediate stage of CO (dehydrogenation). is based on the action of Pd catalysts.

$$HCOOH \rightarrow COOH + H+ + e- \rightarrow CO_2 + 2H+ + 2e-. \quad (1)$$

Eliminating adverse reactions indirect oxidation with the intermediate formation of CO (dehydration):

$$HCOOH \rightarrow CO_{ads} + H_2O \rightarrow CO_2 + 2H+ + 2e–, \quad (2)$$

The Pd composites have a high catalytic activity in the oxidation reactions of the most common types of fuel (hydrogen, formic acid, ethanol, etc.), and are resistant to CO typical catalytic poison to fuel cells [2].

2.3. The Catalytic Properties of Pd Nanocomposites in Hydrogen Isotope Exchange Reaction

The catalytic properties of Pd NP / γ-Al2O3 composites on the base of Pd NP, prepared in reverse micellar solutions by radiation-chemical method were studied in model reaction of homomolecular isotopic exchange of hydrogen. It was found the size effect in the catalytical activity of Pd nanoparticles. It was shown that specific catalytic activity of Pd NP increases with changing of particle size from 1.4 nm to 6.5 nm [3]. The catalytic activity (-196ºC) with increasing nanoparticle size from 1.4 nm to 2.1 nm is increased by 1.7 times, while for NP with size 6.5 nm – only in 3.3 times. Pd NP exceeds activity of the bulk metal more than an order of magnitude.

Nanoscale binary cathode catalysts for direct methanol-oxygen fuel cell prepared on the base bimetallic nanoparticles: Pd/Au, Pd/Pt in the block copolymers of polystyrene and polyvinylpyridine, have very high catalytic activity [5, 6].

2.4. Application and Catalytic Properties of Ruthenium

Ruthenium as well as platinum and palladium, has a catalytic properties, but often differs from them greater selectivity. In heterogeneous catalysis are often used Ru metal and its alloys. The most effective ruthenium catalysts obtained when applying various materials with highly developed surfaces. In many cases it was used together with platinum, in order to increase its catalytic activity. Alloy Rh, Ru and Pt accelerate the oxidation of ammonia in the production of nitric acid. Ru is used for the synthesis of hydrocyanic acid from ammonia, and methane, for getting the saturated hydrocarbons from hydrogen and carbon monoxide. It allows to use ruthenium for the synthesis of a variety of organic and inorganic products. Ru catalyst begins to seriously compete with Pt, Ir and Rh.

Another interesting property of the ruthenium – to absorb / desorb hydrogen – with success can be used to extract hydrogen from gas mixtures and obtain pure hydrogen.

Not to mention the use of radioactive isotopes ruthenium in scientific research, especially at the decision of problems in atomic industry. It is the definitive problems solution of nuclear fuel waste purification from radioactive ruthenium and development of effective ways of extraction of ruthenium from the ore pass through in depth knowledge of the properties and characteristics of this complex and unusual element.

2.5. Rhodium based catalysts

The most important consumer of rhodium-chemical industry. From the platinum and rhodium alloy are made catalyst nets, which at a temperature of 800-900°C led ammonia oxidation to nitrogen oxides - the main stage of the process of nitric acid syntheses. When this is formed as an impurity CO, which is a poison to fuel cells. Accordingly, there is a problem of selective CO oxidation. To resolve this problem are used patterns based on Pt-Rh systems.

Rhodium catalyst in the carbon media is used for chemical current sources (hydrogen electrode). One of the problems impeding the commercialization of hydrogen technologies is the high cost of electrochemical converters and, including through the use of metals of platinum group (MPG) as catalysts.

Using rhodium catalyst allows to combine enzymatic and metal-complex catalysis in a single molecule. Japanese scientists developed a catalyst that successfully combines high catalytic activity of rhodium complexes, and high selectivity of enzymatic catalysis. Rhodium, platinum and palladium are the basis for most active catalysts used in thin and industrial organic synthesis. However, the nature does not discovered enzymes, active centers which would work through these metals. Artificial ferment catalysts created using rhodium and other metals of 8-10 groups, could fundamentally change the approach to high-performance, highly selective catalysis.

Alloys of platinum with 1-3% rhodium go for the manufacture of chemical laboratory ware, which require high chemical and thermal resistance and ability to change your weight, even after prolonged annealing.

2.6. Electrocatalysts for Anodes and Cathodes

Platinum has not enough activity for use in fuel cells in the direct alcohols oxidation. Therefore, been investigated by a number of binary and ternary catalysts based on it. In the framework of bifunctional mechanism promoting metal should provide the adsorption of oxygen-containing particles at low voltages. In addition, the promoting metal should have sufficient stability and not slow down the rate of absorption and dehydrogenation of methanol. Among the binary systems PtM were investigated Sn, Bi, Mo, Ru, Os, Ir. During the formation of more complex systems, attempts were made to use refractory metalls Zr, Nb, W, Mo or their oxides. Despite a significant number of works dedicated to the development of anode catalysts, at the present time it is generally recognized that the most acceptable electrocatalytic system is PtRu [10]. The catalytic effect takes place for different types PtRu systems: alloys, electrolytic precipitation, deposition platinum ruthenium different methods, in the deposition of Pt microquantities on dispersed Ru. Despite the ongoing debate on the optimal design of these systems, the most important condition of electrocatalytic effect is the existence of a developed contact boundary Pt/Ru.

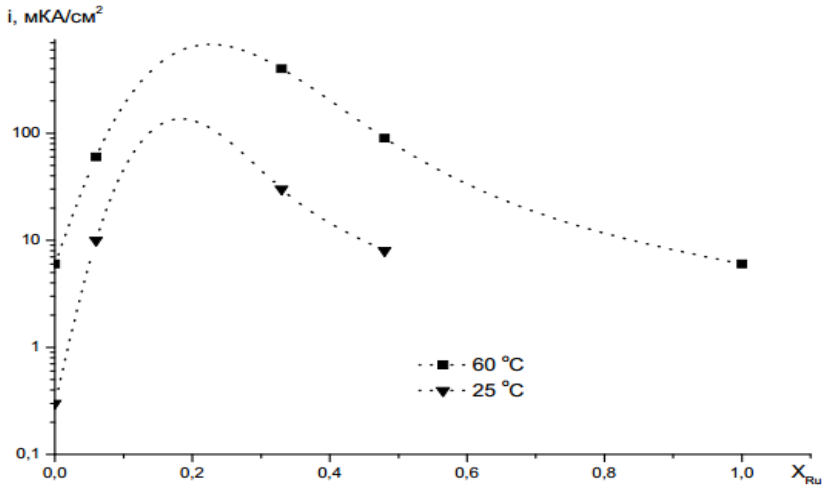

Fig1.1. *Dependence of oxidation rate of 0,5M methanol in 0.5M H_2SO_4 on composition Pt/Ru alloy at various temperatures.*

3. EXPERIMENT METHODOLOGY

3.1. Radiation-Chemical, Radchem, Synthesis of Metal Nanoparticles

The radiation–chemical synthesis of metal NPs is based on the reduction of metal ions in reacting with hydrated electrons (e_{aq}^-) or other reducing radical particles generated by ionizing radiation (γ-rays of ^{60}Co) in a water–organic reverse micellar solution of Me^{n+}/H_2O/AOT/isooctane. Stable nanostructure particles are formed in a water pool of reverse micelles as a result of the subsequent agregation of atoms and metal ions. The radiation dose was 1÷5 Mrad (10÷50 kGy).

1. The selected method of radiation-chemical reduction of metals ions (Revina A.A. 2006) allows to obtain stable metal nanoparticles and has a number of essential advantages [7]:
2. The reduction of metal and formation of nanoparticles in micelles, in an organized environment, contributing to the formation of nanostructured agregates and their stabilization;
3. The shell micelles creates certain restrictions for the growth of these units, allowing to produce particles with small size, because the reaction of reduction and formation of nanoparticles in water pool;
4. Setting the size of the water pool of micelles it can be possible to influence on size of nanoparticles;
5. The shell of micelles prevents the agregation of nanoparticles, so they can long time remain in solution without losing its high specific properties;
6. Application of reverse micellar solutions allows to use the optical measurement for detection of nanoparticles, detection of their concentration change during storage time, due to adsorption of particles in contact with various materials. [8]

3.2. Chemical Reduction, Chem, of Metal Ions and Nanoparticles Formation

In order to synthesize nanoparticles, we used reverse micelle solutions and the same compounds as for radiation-chemical synthesis. As reducers for Me ions, polyphenol compounds—flavonoids—were introduced: quercetin (3, 5, 7, 3', 4'-pentahydroxyflavone) in 0.15M AOT/isooctane solution.

Pouring aqueous solution with Ru atoms in reverse micelle solution quercetin/0.15M AOT/isooctane and stirring in conical flasks colors it typical of Me nanoparticles; the latter enables us to apply spectrophotometry in studying the formation of Me nanoparticles and their content in accordance with the time, temperature, and other parameters.

Chemical reduction [15, 16, 17] of Me ions proceeds under aerobic conditions, whereas radiation-chemical reduction occurs under anaerobic ones. In order to increase the yield of reducing agents in radiolysis, we added isopropanol (no more than 0.02 M), which is an acceptor of oxidizing radicals OH [1].

The reagents

1. AOT-[bis(2-ethylhexyl) sulfosuccinate sodium]
2. 3,5,7,3',4'-pentoksiflavone (quercetin)
3. solvent (isooctane)
4. isopropyl alcohol
5. complex dichloride tetraamminepalladium
6. solution $Ru(OH)Cl_3$ 0,04 M
7. solution $RhCl_3*4H_2O$ 0,04 M
8. distilled water.
9. inert gases (Ar, He)
10. a nanocomposite of γ-Al_2O_3 carrier (brand "trilistnik") with nanoparticles of metalls deposited from micelle solutions

The scheme reverse micelles:

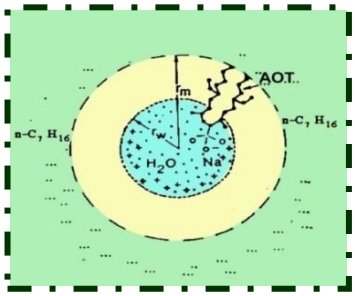

Solubilization coefficient, $\omega_0 = [H_2O] / [AOT]$.

AOT-[bis (2-ethylhexyl) sulfosuccinate].

3.3. Preparation of Reverse Micellar Solutions

Preparation of reverse micelle solutions for the synthesis of Me NPs using various methods for reduction of the metal ion. The appropriate amount of an aqueous solution of the required concentration according to the chosen degree of hydration ω, where ω is the water to AOT molar ratio in the reverse micelle solution: ω = [H2O]/[AOT], was added to a 0.15M solution of the surfactant (AOT). The concentration of rhenium ions in the micelle water pool remained constant, [Me]wp = const, depending on the chosen initial concentration of the salt, whereas the ion concentration in the reverse-micelle solution increased in proportion to the ω value, i.e., $[Me]_{RMS} \sim \omega$ [1].

The saturation of the solution by argon lasted for 30 - 40 minutes. After that, the cell with a solution was hermetically sealed and put on irradiation [12].

3.4. The Source of Ionizing Radiation, Dosimetry

For irradiation of the samples used in radiation and chemical installation RKHM-g-20 (MUCTR them. D.I. Mendeleev). Dose rate 0,111 Gy/sec (RHM-γ-20), which was determined using a dosimeter Fricke.

3.5. Experimental Methods of Nanoparticle Investigations

3.5.1. The optical method

Optical absorption spectra were measured by using of Spectrophotometr HITACHIU-3310 (from 190 nm to 900 nm) concerning the solution of AOT/isooctane in the presence of oxygen. Optical path length quartz cell 1.0 mm.

The spectra of optical absorption (electron plasmon resonance, EPR) of metal nanoparticles in the reverse micellar solutions were measured on depending on the metal nature, the concentration of metal and their ratio (for bimetallic), doses of radiation, and storage time after exposure. As reference solution was selected the reverse micellar solution, RMS, (0.15M/AOT/isooctane) and temperature, T_{room}.

Emission spectra were measured from 190 nm to 900 nm (Hitachi F 7000 spectrofluorimetr) in reference to the solution of AOT/isooctane in the presence of oxygen. Optical path length quartz cell 1.0 cm; the wavelength of excitation was 280 nm [11].

3.5.2. The electrical and catalytic activity of nanocomposites

3.5.2.1. Preparation of Modified Electrodes

Directly on the surface of disposable planar electrodes inflicted 20 ml of dispersion of the sample, wherein the drop must not fall on a polymer base electrode. The electrode surface is dried in a stream of inert gas Ar (argon 99.99%) before full drying (drying of the electrode takes at least an hour). The evaluation criteria applied layer of catalyst - visual. Then the surface of the electrode is repeatedly washed with water-alcohol solution (for treatment of reverse micelles) and then dried in argon stream.

3.5.2.2. Electrocatalitical Measurements

We use only fresh prepared electrolyte, prepared on the day of measurement - 0.5M H_2SO_4. Impurities in the electrolyte can distort the voltamperometric, V/A, data.

The cleanness of the electrochemical cell is very important because can be adsorbed various impurities. Therefore, it is necessary once in 3-4 days to wash cell by boiling in the solution - H_2O_2:H_2SO_4:H_2O=15:1:75. The auxiliary electrode was hydrogen electrode, it needs to be recharged every 2-3 days. The chlorine-silver electrode was reference one.

As working electrodes were chosen disposable planar electrodes because of metal nanoparticles is difficult to be desorbed from surface of used electrode. Measurement of catalytic activity was conducted using a potentiostat-galvanostat Intelligent Potentiostatic Control - Pro MF (Russia) with the software IPC2000.

Before measurement of voltamperometry we need to spend 10-15 "blank" cycles on average scanning speed (100mV/c) for the output of the electrode to normal working mode, which confirms the cleanness of surfaces. The scan speed can be increased, for acceleration of the process up to 300mV/c.

3.5.2.3. Calculation of the Catalyst Characteristics

On the base of the cyclic voltamperometric data were calculated basic electrochemical characteristics of catalysts - specific electrochemically active area of catalyst (ESA) relatively to hydrogen and oxygen and the average particle size of catalyst (d). Using voltamperometry, calculate the space under the peaks oxygen reduction Q_{O2}, peak of reduction (adsorption) hydrogen Q_{adsH2} and peak oxidation (desorption) hydrogen Q_{desH2}. Knowing the area under these peaks (μc) and the constants of the charge density Q_X needed to restore the monolayer oxygen (420 μc) and hydrogen on platinum (220 μc), the area of nanocatalyst was calculated:

$$S = \frac{Q}{Q_X} \times 10^{-4}, \text{ m}^2 \quad (1)$$

Knowing a portion of the sample m (20 μg) and the percentage of investigated nanoparticles X, a specific electrochemically active area was calculated:

$$ESA = \frac{S}{m \cdot X}, \text{ m}^2/\text{g} \quad (2)$$

The average particle size was calculated on the base of assumption that the particles have spherical form:

$$d = \frac{6}{ESA \times \rho}, \quad (3)$$

where p is the density of the catalyst.

3.5.3. Method of Measurement of Nanosized Particles of Metals by Atomic-Force Microscope (AFM)

The basic instrument in the present work was atomic force microscope EnviroScope Veeco Instruments (USA).

Technical characteristics:

- Resolution along the X-Y axis: 0.15 nm, along Z-axis: 0.1 nm,
- Ability to work in a high vacuum.

4. EXPERIMENTAL RESULTS AND THEIR DISCUSSION

4.1. Optical absorption spectra of nanoparticles of Pd, Ru, Rh

Optical absorption spectra of nanoparticles of Pd, Ru, Rh (c ~ ω) on intensity of optical absorption are presented in Fig. 3.1 for Pd on Fig. 3.2 for Ru(1), Rh(2).

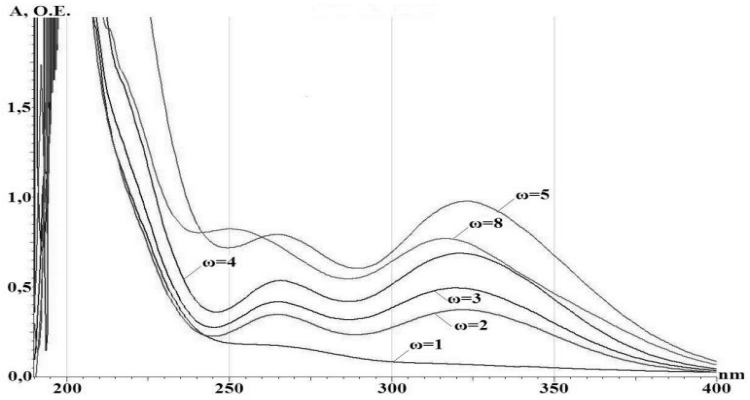

Fig3.1. *The optical absorption spectra of Pd nanoparticles in RMS with different values of ω*

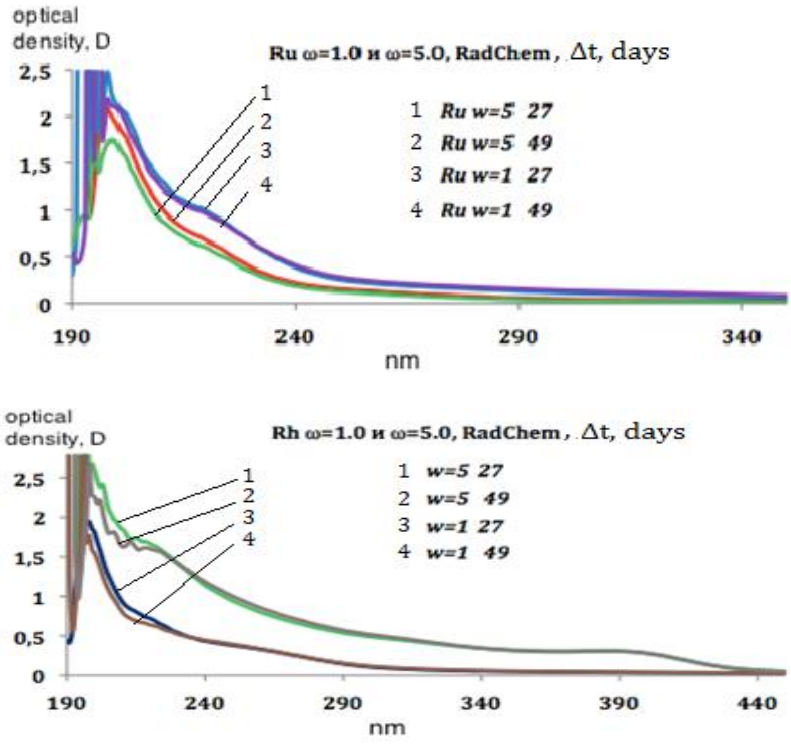

Fig3.2. *The optical absorption spectra of nanoparticles Ru (1) and Rh (2). Dose 15 kGy.*

Table 3.1. *The typical peaks on the optical absorption spectra of Pd, Rh, Ru NPs in RMS*

Pd RadChem	Ru RadChem	Rh RadChem
λ, нм		
265	218-225	214-223
323	-	260-270
-	-	390

Fig. 3.1 and 3.2 illustrates that Pd, Rh, Ru NPs mainly have peaks of optical absorption (plasmon resonance) in the UV range. The shape of the spectrum, their intensity, under other equal conditions, depend on the nature of metal. As illustrated in the following figures, the nature of changes in the form and intensity of optical absorption bands in the process of storage of the samples also depends on the nature of the metal.

The change of the optical characteristics of Pd nanoparticles in RMS, depending on the time of storage of the samples illustrated in figure 3.3.

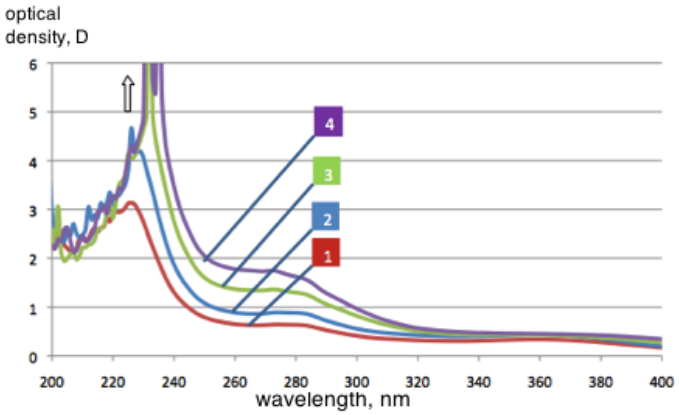

Fig3.3. *optical absorption spectra of Pd nanoparticles, Δt, days, after synthesis - 1, after 150 - 2, 247 - 3, 310 days - 4.*

Table3.2. *The change in the optical density, OD, at selected wavelengths Pd nanoparticles during storage of samples for Δt after synthesis.*

Wavelength, nm	200	226	255
OD Pd	2.22	3.14	0.70
OD Pd after 150 days	2.97	4.66	0.95
OD Pd after 247 days	2.61	4.20	1.42
OD Pd after 310 days	2.41	4.30	1.80

Data resulted in table 3.2 illustrates the rise in the intensity of optical absorption after synthesis. Analysis of this spectrum in the area from λ=220 nm to λ=330 nm peak at λ=228 nm has shifted in the long-wave region of about 10 nm, which is probably connected with the agregation of the particles. The increase in optical density with time storage of nanoparticle solutions confirms their high stability.

Influence dose of radiation on the formation of Pd NPs illustrated in Fig. 3.4.

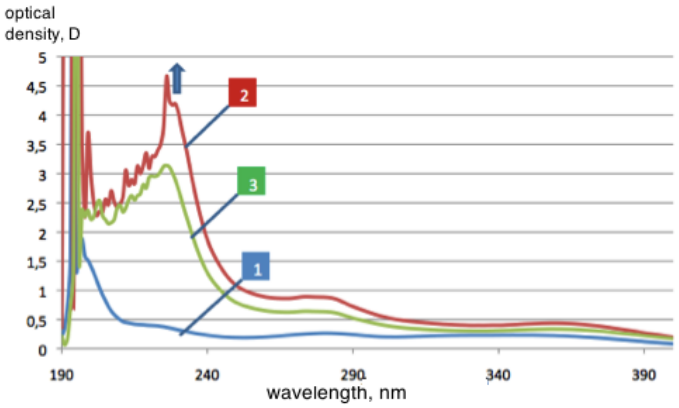

Fig3.4. *The optical absorption spectra of RMS of Pd NPs at irradiation doses, kGy: 1 - 15, 2 - 18, 3 - 27.*

Dependence (Fig. 3.4) spectra Pd NPs from the dose of radiation during the synthesis shows that lower the optical density of the spectrum are the solutions of the particles formed at high dose (27 kGy) than at a dose of 18 kGy. Apparently at high doses is some degradation of nanoparticles. Synthesis at the dose of 15 kGy leads to the formation of nanoparticles smaller size, which absorb more short-wave region of the spectrum, but the peaks of the strips in λ=230 nm and λ=280 nm, are present.

On the other hand, spectrum in the UV has poor resolution to conclude the acquisition of smaller particles.

4.2. Luminescent analysis of RMS of NPs

The influence of rhodium NPs on the luminescence AOT/isooctane is illustrated on Fig. 3.8.

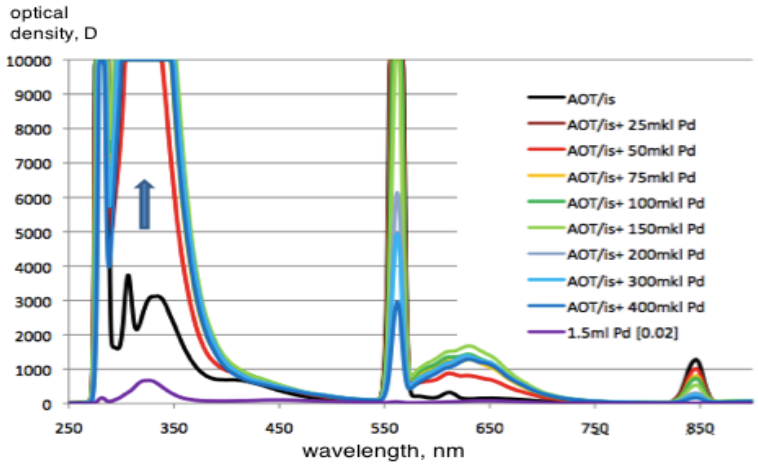

Fig3.8. *Impact of concentration Pd NPs on the luminescence AOT/isooctane. Wl=280 V=700. Dose 18 kGy.*

Analysis figure 3.8 is illustrated that the Pd NPs show a strong increase luminescence AOT/isooctane, but if maximum concentrations observed the effect of quenching of luminescence.

The impact of Ru NPs on the luminescence AOT/isooctane is illustrated in Fig. 3.5-3.6.

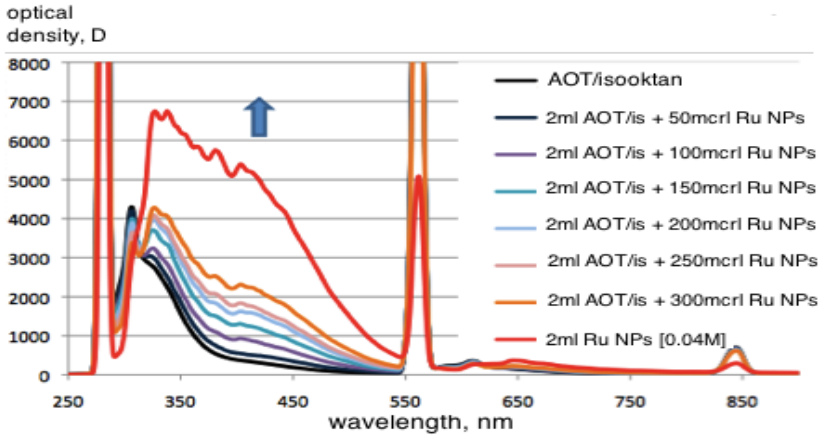

Fig3.5. *Impact of Ru NPs on the luminescence AOT/isooctane.*

Figure 3.5 illustrates that relatively luminescence solution AOT/isooctane increase the maximum luminescence occurs in proportion to the increase of nanoparticles, up to the maximum.

Analyzing spectra of luminescence shown in figures 3.5 and 3.6, we can conclude that the activity increase of luminescence AOT/isooctane Ru nanoparticles for five months has increased noticeably. But with the maximum concentration of ruthenium [M] there is a reverse effect, almost complete quenching of luminescence lamps 280 and 560 nm nm and the formation of a broad peak (from 300 to 550 nm). This fact can talk about the concentration effect on the luminescence received particles and their change over time, as evidenced by changes in the spectra of optical absorption.

On Fig. 3.7 is illustrated the influence of rhodium nanoparticles on the luminescence AOT/isooctane.

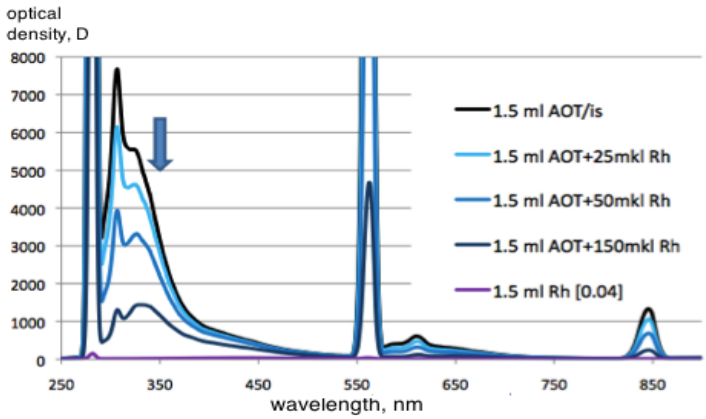

Fig3.7. *Impact of concentration Rh NPs on the luminescence AOT/isooctane.*

Luminescence spectra of rhodium nanoparticles is illustrated on Fig. 3.7 show luminescence quenching of AOT/isooctane, during five months the activity of fighting increased.

4.3. AFM Image of the Nanoparticles

The synthesis was carried out by using 0.15 M solution AOT/isooctane, w=5.0, dose 18 kGy. Total coefficient of solubilization w=5.0. The concentration of metal ions in the initial solution of Ru and Rh salt was 0.04 M; for Pd - 0.02 M.

AFM image Pd nanoparticles are presented on Fig. 3.9; The size of NPs (dose of 15kGy), the average size of the NPs from 0.8 to 5.5 nm

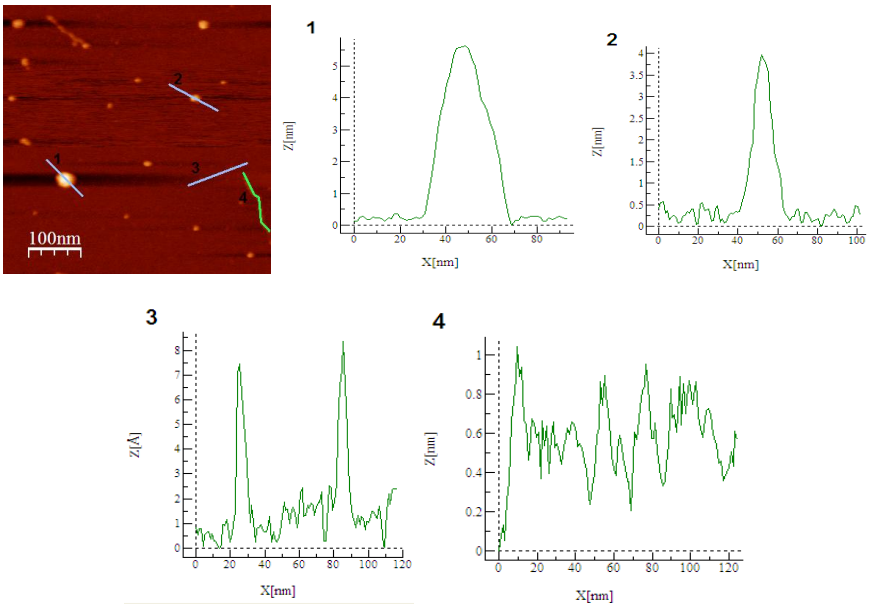

Fig3.9. *AFM image, and topographic segment of the selected zone for Pd nanoparticles.*

AFM image of Rh nanoparticles are illustrated in Fig. 3.10; the size of nanoparticles (dose of 15 kGy), the average size of nanoparticles from 0.6 to 1.2 nm.

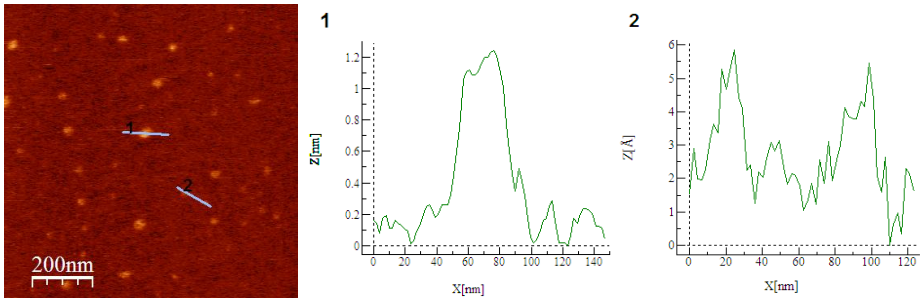

Fig3.10. *AFM image, and topographic segment of the selected zone for Rh nanoparticles.*

Fig. 3.11 illustrate the AFM image of Ru nanoparticles; the size of nanoparticles (dose of 15 kGy), the average size of nanoparticles from 1 to 3 nm.

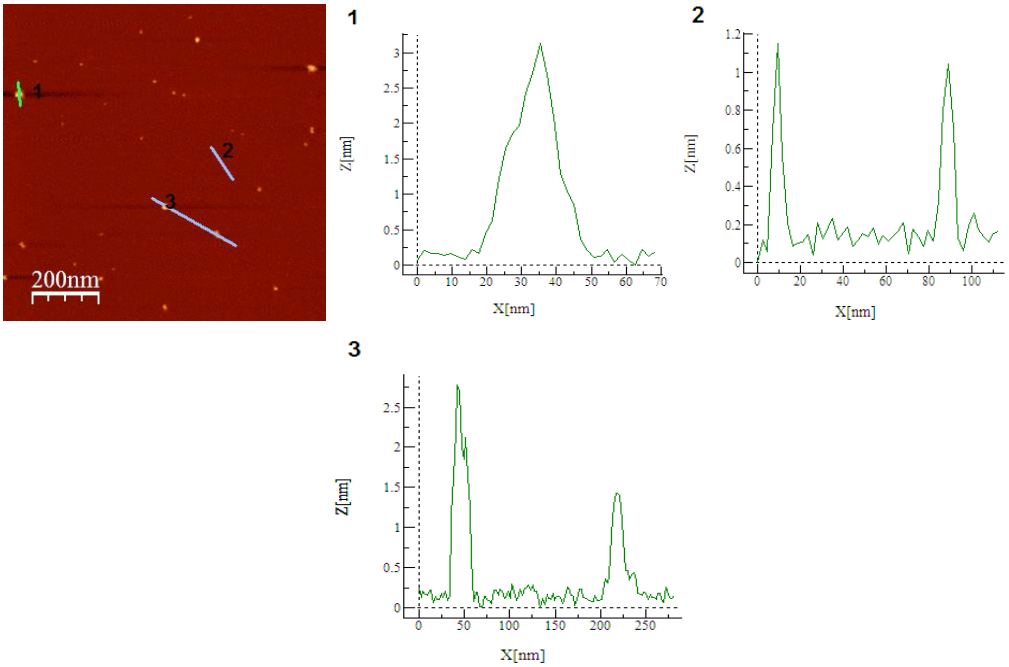

Fig3.11. *AFM image, and topographic segment of the selected zone for Ru nanoparticles .*

Table3.3. *The average size of ruthenium and rhodium nanoparticles. AFM research.*

Ru NPs		Rh NPs		Pd NPs	
Characteristic	The average size of nanoparticles, along the axis Z, nm	Characteristic	The average size of nanoparticles, along the axis Z, nm	Characteristic	The average size of nanoparticles, along the axis Z, nm
ω=1.0 Chem Qr	3,5-5	ω=1.0 Chem Qr	2,5	ω=5.0 RadChem, 18 kGy	1-10
ω=5.0 Chem Qr	4-5	ω=5.0 Chem Qr	3-4		
ω=1.0 RadChem	2-6	ω=1.0 RadChem	2-4	ω=5.0 RadChem, 15 kGy	0,8-5,5
ω=5.0 RadChem	3,5-6	ω=5.0 RadChem	2-4		

At synthesis at a lower dose of radiation reverse micellar solutions particles are synthesized with a smaller size. The increase of radiation dose leads to the formation of nanoparticles with more diameter and large deviation nanoparticles in size, there are found large agregations d>40 nm.

4.4. Electrical and Catalytic Properties of Nanoparticles

The synthesis was carried out in reverse micellar solutions of 0.15 M AOT/isooctane, w=5.0 when the concentration of metals in the initial solution: [Ru] and [Rh] = 0.04M; [Pd] = 0.02M. Synthesis was carried out at the dose of 15 kGy. For bimetallic particles ratio 1:1, total fertility rate of solubilization w=5.0. Spectra were measured relative to the AOT/isooctane.

Comparison of CVA disposable electrode and electrode coated with nanoparticles Pd (Fig. 3.12), Rh (Fig. 3.13), Ru (Fig. 3.14) in 0.5M H_2SO_4.

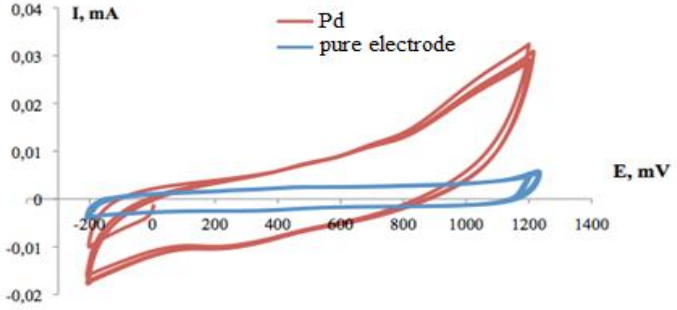

ESA = 33,9 m2/g, d = 14 nm.

Fig3.12. *Comparison of CVA disposable electrode and electrode coated with a solution of Pd (ω = 5) in 0.5M H_2SO_4.*

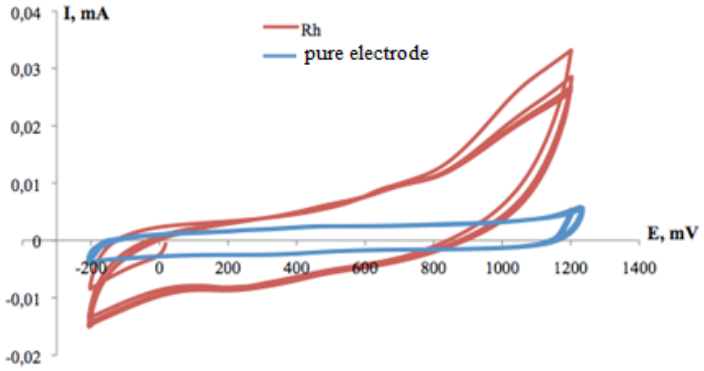

ESA = 23,9 m2/g, d = 20 nm.

Fig3.13. *Comparison of CVA disposable electrode and electrode coated with a solution of Rh (ω = 5) in 0,5M H_2SO_4.*

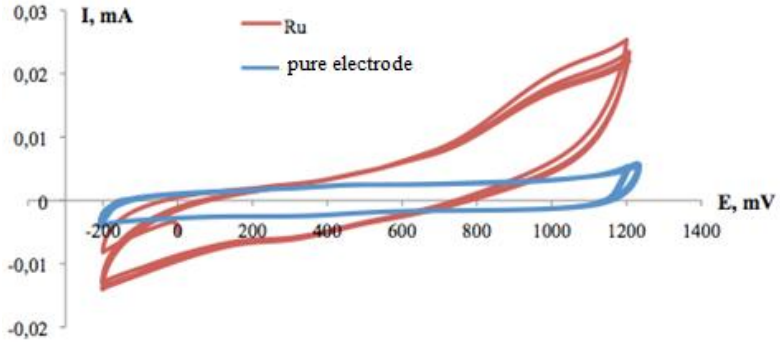

ESA = 36 m2/g, d = 13,6 nm.

Fig3.14. *Comparison of CVA disposable electrode and electrode coated with a solution of Ru (ω = 5) in 0,5M H_2SO_4.*

Table3.4. *Comparing the current values (oxygen branches) for nanoscale*

Nanoparticles	ω	Metal concentration in solution	I, мА
Pd	5	0,27 мМ	0,010
Ru	5	0,54 мМ	0,09
Rh	5	0,54 мМ	0,002

Current value modulo (minus sign is ignored), because the process of removing CVA - reversible process, and oxygen and hydrogen comparable values. In this case were compared trends of process oxygen in the field of recovery. The measurement results electrocatalytic activity not shown in the table, because due to small concentrations of nanoparticles of activity values are very small.

Influence of additives second metal is easy to see from data of table. Separately Ru and Rh nanoparticles show the small currents recovery. However, with the addition of Pd (if to compare the pure Rh and Pd/Rh) current bimetal increased almost 5-fold, which suggests undeniable advantage of similar composition in the catalytic process. The difference between Pd and one-component bimetallic Pd/Ru practically invisible. It should be noted that the creation of nanoparticles with the use of palladium improves all properties of nanocomposite.

4.5. Determination of Nps Absorbption Properties

For determination of the active surface of the nanocomposites, which were prepared with Al_2O_3, we use process of hydrogen adsorption at -196°C. Were built adsorption isotherms, i.e. the amount of adsorbed hydrogen from residual pressure (Fig. 3.14). In the form of isotherms to judge the type of adsorption: the obtained results suggest that the observed sample chemisorption of hydrogen. Adsorption isotherms have pronounced plateau, which is the monolayer chemisorbed hydrogen. On the same graph plotted the results of re-hydrogen adsorption after the evacuation of the sample at the same temperature (-196°C). From the data presented, we conclude that the whole adsorbed on Ru hydrogen weakly associated with the surface and is easily removed by pumping diffusion pump.

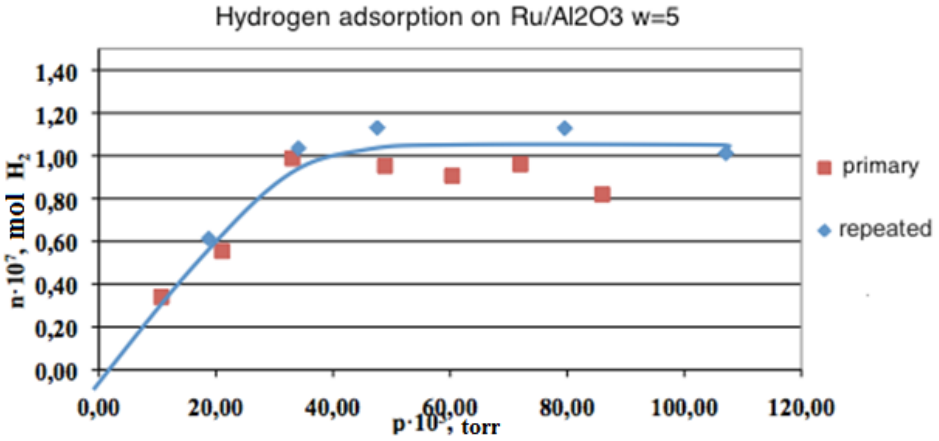

Fig3.14. *Isotherm of adsorption of hydrogen for sample Ru/Al2O3 mass m=0.07g*

In table 3.5 is illustrated the values of the active surface S, sm^2, calculated on the obtained isothermal adsorption, as well as the value of the specific active surface Sud, sm2/g for a sample of a catalyst.

Table3.5.

m, г	**S, см^2**	**$S_{уд}$, sm^2/g**	C_{Ru}, mass.%	σ_{Ru}, surf.%	D_{Ru}, %
0,07	**75**	**1070**	**0,032**	**0,049**	**25**

It is calculated that the content of metallic Ru planted from the solution should be 0.14% (mass). Knowing the monolayer volume of hydrogen and weight, we can calculate the percentage of metal on the surface of the sample relative to the mass of a sample (C_{Ru},%), the share of surface occupied by metal (σ_{Ru}, a surface.%) and the dispersion of metal (D_{Ru}).

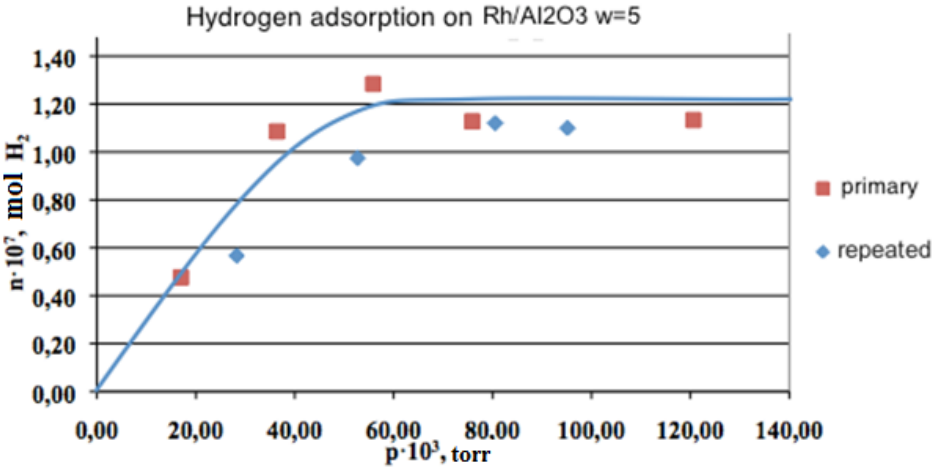

Fig3.15. *Isotherm of adsorption of hydrogen for sample Rh/Al2O3 mass m=0.07 g*

Table 3.6 presents the values of the active surface S, sm2, calculated on the obtained isothermal adsorption, as well as the value of the specific active surface Sud, sm2/g for a sample of a catalyst.

Table3.6

m, г	S, см^2	$S_{уд}$, см^2/г	C_{Ru}, mass.%	σ_{Ru}, surf.%	D_{Ru}, %
0,07	82,5	1178	0,035	0,054	25

4.6. Comparison of Catalytic Activity of Supported Catalysts Based on Nanoparticles of Ruthenium and Rhodium with Other Catalysts on the Basis of These Metals

On Fig. 3.16 and 3.17 are illustrated the comparison of catalysts on the basis of ruthenium and rhodium obtained in various ways:

- From oratorically systems,
- Traditional method of impregnation [12]
- The deposition of films in vacuum [13].

From figures are visible to the following pattern:

1) With different methods of application of ruthenium and rhodium in the study of evaporated in vacuum films temperature dependence of specific catalytic activities have been varied. For samples Rh from micellar solution, Rh_{mic}/Al2O3 and Rh, impregnating obtained, Rhprop/Al2O3 there are two temperature ranges with different values of activation energy (Elt ~ 0 kJ/mol, Eht = 5.1 kJ/mol and the Elt= 1.6 kJ/mol, Evt= 3.9 kJ/mol, correspondingly). Film Rh in the interval of temperatures from-S to-700C have a constant value of activation energy equal to the CNT = 1.3 kJ/mol. For samples Ru_{mic}/Al2O3 temperature dependence Kud is the breaking and is divided into two temperature ranges with different values of activation energy (Elt~0 kJ/mol, Eht~9 kJ/mol). For the catalyst, obtained by the traditional method of impregnation with subsequent restoration of metal, 0.5% Ru_{prop}/Al2O3 observed the same character based cluck on the temperature, however, the break point is shifted towards a more positive temperatures (Elt = 0.5 kJ/mol, Eht~ 9 kJ/mol). Ru film obtained by thermal spraying in high vacuum, studied in less wide temperature range. In the interval of temperatures from -1960C to -1400C activation energy isotopic exchange of hydrogen on films ruthenium constant and is set Elt = 2.5 kJ/mol.

2) Catalytic activity Ru_{mic}/Al2O3 in the low temperature range coincides with catalytic activity Ru_{prop}/Al2O3. At high temperature catalytic activity Ru_{mic}/Al2O3 exceeds the catalytic activity Ru_{prop}/Al2O3 approximately 16 times. It should be noted that in previous works [12, 13], it was shown that the catalyst 0.5% Ru_{prop}/Al2O3 showed the highest specific catalytic activity among all investigated caused impregnating catalysts on the basis of transition metal Rh, Pt, Ni, Pd. Thus, we can say that the obtained composite system based on nanoparticles ruthenium is also the most active in this isotope exchange reaction of hydrogen. The catalytic activity Rh_{mic}/Al2O3 in the whole range of temperature exceeds the catalytic activity Rh_{prop}/Al2O3: at -196^{0}C approximately by 5 times, at 0C - in 10 times.

3) At a temperature -196^{0}C catalytic activity of Rh NPs slightly exceeds the catalytic activity of the ruthenium films. When the temperature drops below -196^{0}C nanoparticles becomes more active films rhodium, and the lower the temperature, the higher their activity compared with net rhodium (due to the differences in the values of activation energy).

Thus, in the paper the results of high-active catalytic systems based on nanoparticles of ruthenium and rhodium in the reaction H2-D2 exchange. Research has shown, that at temperature -196^{0}C the catalyst on the basis of nanoparticles ruthenium have the same catalytic activity with films ruthenium. When the temperature drops below -196^{0}C nanoparticles becomes more active films ruthenium, and the lower the temperature, the higher their activity compared with net ruthenium (due to the strong differences in the values of activation energy).

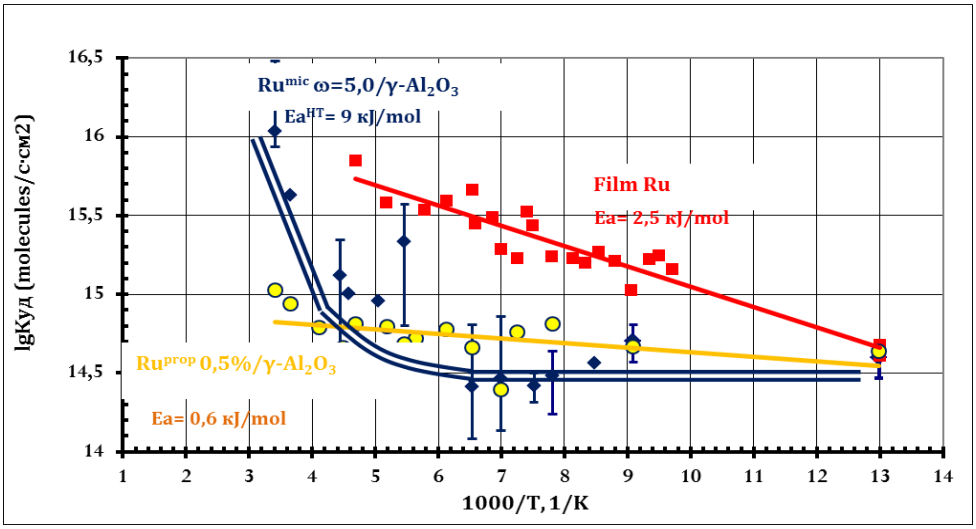

Fig3.16. *Comparison of the dependencies of specific catalytic activity on temperature for the samples 0.5% Ru_{prop}./ Al2O3, Ru film and Ru_{mic}/Al2O3 ω=5.0.*

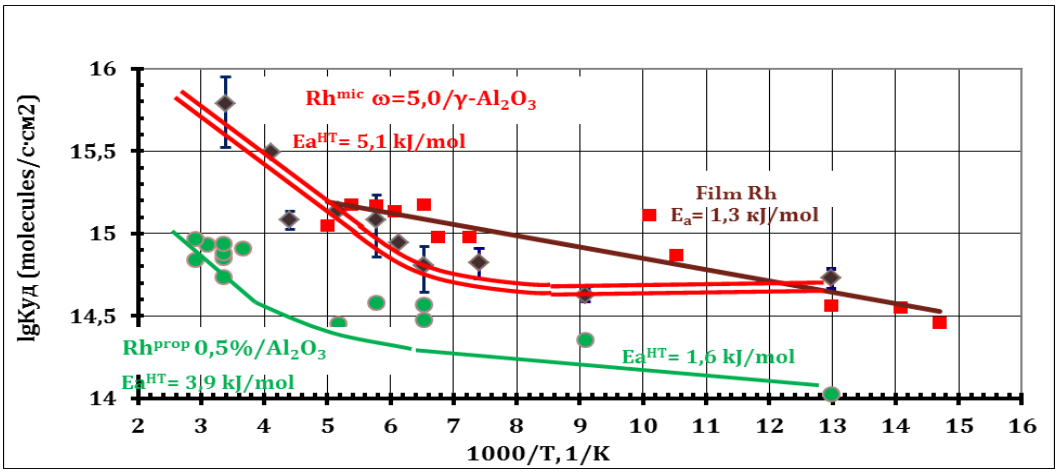

Fig3.17. *Comparison of catalytic activity Rh_{mic}/Al2O3 ω = 5.0, 0,5% Rh_{prop}/Al2O3 Rh film.*

5. CONCLUSION

1. Stable nanoparticles of metals: Pd, Ru, Rh synthesized by the radiation-chemical method in reverse micellar solutions.
2. The method of optical spectrophotometry investigated the formation of the metal nanoparticles, depending on the dose, the nature of the metal, concentration and time of storage of samples.
3. The measure of the luminescence reverse micellar solutions of metals NPs allowed to assess the impact of radiation dose, the nature of the metal, the concentration of metal ions and storage time of the samples on the optical characteristics of nanoparticles is mainly in the nature of luminescence extinguishing solution 0.15M AOT/isooctane.
4. Found that Rh NPs in all experiments stew luminescence solution AOT/isooctane, while Ru NPs raise the intensity of luminescence band solution AOT/isooctane and appears peak own luminescence of Ru NPs in the field ($\lambda_{макс}$ = 320 nm).
5. Held adsorption nanoparticles of ruthenium and rhodium on the carrier surface γ-Al_2O_3
6. Studied the catalytic activity of nanocomposites based on γ-Al_2O_3 containing ruthenium and rhodium nanoparticles, isotope exchange reaction in molecular hydrogen.
7. Discovered the influence of size effects nanostructures in catalytic activity of ruthenium and rhodium nanoparticles.
8. It is shown that particles have high catalytic activity in a wide range of temperatures from 77K to 300K.

REFERENCES

[1]. Revina A.A., Kezikov A.N., Larionov O.G., Dubinchuk V.T. Synthesis and physico-chemical properties of stable palladium nanoparticles // Russian chemical journal. 2006. T.50. № 45. P.55-60.

[2]. Yashtulov N.A., Gavrin S.S., Revina A.A. Flid V.R. Formation of nanocomposite catalysts palladiyana porous silicon anodes for fuel cell // Proceedings of the Academy of Sciences. Chemical series. 2010. T.59. №8. P. 1450-1455.

[3]. Sergeev M.O., Antonov A.Yu., Odintsov A.A., Zhavoronkova K.N., Revina A.A., O.A. Boeva. The catalytic properties of composite systems based on palladium nanoparticles in hydrogen isotope exchange reaction // Advances in chemistry and chemical technology. T.26. №7. P.24.

[4]. Greenberg V.A., Mayorov N.A., A.A. Pasynskiy. Pt-Sn-nano electrocatalysts direct destructive oxidation of ethylalcohol // Electrochemistry. 2009. T.45. №12, P.1427-1433.

[5]. Yashtulov N.A., Gavrin S.S., V.P. Bondarenko, Kholostov K.I., Revina A.A., Flid V.R. Formation of platinum nanocomposite catalysts on porous silicon // Izv. RAN. Ser. chem. 2011. T.60. №3. P.425-430.

[6]. Tsivadze A.Y., Tarasevich M.R., Bogdanovskaya V.A., L.N. Kuznetsova, Kapustin N.A., Modestov A.D. Modified binary cathode catalysts for direct methanol-oxygen fuel cell // Doklady Sciences. 2006. T.410. №2. P.203-206.

[7]. M.Scherbina. «Secret Files of the catalysts of life». Journal of Science, Lawrence Berkeley National Laboratory.

[8]. News chemistry. «Enzymatic and metal complex catalysis water molecule». Organic& Biomolecular Chemistry, 2006, 4, 3571.

[9]. Mosin O.V. Nanotechnology and incorporation of deuterium , oxygen -18 , carbon -13 and nitrogen -15 in the amino acid molecules and proteins // Journal «Samizdat» : Natural History

[10]. 10 . Ivasita T., Vielstich W., Lamm A., Gasteiger H.A. In Handbook of Fuell Cell. John Willey and Sons, 2003 . Vol. 2 , P. 603.

[11]. Parker S. Photoluminescence solutions. - New York: Wiley, 1972 – P.511.

[12]. O.S. Bystrova. «Low-temperature hydrogen isotope exchange gomomolekular on catalysts with deposited transition metals». PhD thesis. MUCTR. D.I. Mendeleev, 2008.

[13]. L.S. Kharitonov. «Study of hydrogen isotope exchange reaction on ruthenium catalysts». Thesis. MUCTR. D.I. Mendeleev, 2005.

[14]. Patent RF 18.11.04. № 2270831. Revina A.A., Kozlov A. I., Kezikov A.N., Magomedbekov E.P.

[15]. Larionov, O.G., Revina, A.A., Belyakova, L.D., et al., Prot. Met. Phys. Chem. Surf., 2011, vol. 47, no. 6, p. 748.

[16]. Egorova E.M. and Revina A.A., ColloidsSurf., A,2000, vol. 168, p. 87.

[17]. Revina A.A., Prot.Met.Phys. Chem. Surf., 2009, vol.45, no. 1, p. 54.